

5. COMPOSITION AND PROVENANCE OF TURBIDITE SAND AND HEMIPELAGIC MUD IN NORTHWESTERN CASCADIA BASIN¹

Michael B. Underwood² and Kimberly D. Hoke²

ABSTRACT

Sequences of late Pliocene to Holocene sediment lap onto juvenile igneous crust within 20 km of the Juan de Fuca Ridge in northwestern Cascadia Basin, Pacific Ocean. The detrital modes of turbidite sands do not vary significantly within or among sites drilled during Leg 168 of the Ocean Drilling Program. Average values of total quartz, total feldspar, and unstable lithic fragments are $Q = 35$, $F = 35$, and $L = 30$. Average values of monocrySTALLINE quartz, plagioclase, and K-feldspar are $Q_m = 46$, $P = 49$, and $K = 5$, and the average detrital modes of polycrystalline quartz, volcanic-rock fragments, and sedimentary-rock plus metamorphic-rock fragments are $Q_p = 16$, $L_v = 43$, and $L_{sm} = 41$. Likely source areas include the Olympic Peninsula and Vancouver Island; sediment transport was focused primarily through the Strait of Juan de Fuca, Juan de Fuca Channel, Vancouver Valley, and Nitinat Valley. Relative abundance of clay minerals (<2- μ m-size fraction) fluctuate erratically with depth, stratigraphic age, and sediment type (mud vs. turbidite matrix). Mineral abundance in mud samples are 0%–35% smectite (mean = 8%), 18%–59% illite (mean = 40%), and 29%–78% chlorite + kaolinite (mean = 52%). We attribute the relatively low content of smectite to rapid mechanical weathering of polymictic source terrains, with little or no input of volcanic detritus from the Columbia River. The scatter in clay mineralogy probably was caused by converging of surface currents, turbidity currents, and near-bottom nepheloid clouds from several directions, as well as subtle changes in glacial vs. interglacial weathering products.

INTRODUCTION

Leg 168 of the Ocean Drilling Program (ODP) was designed to document several fundamental aspects of hydrothermal circulation across the eastern flank of Juan de Fuca Ridge (Fig. 1), including: (1) the influence of basement topography, sediment thickness, and sediment permeability on thermophysical characteristics of fluid circulation; (2) the sensitivity of fluid composition to crustal age, temperature, and degree of sediment burial; (3) the nature and causes of physical, mineralogic, and chemical alteration of the igneous crust with increasing age and depth of burial; and (4) heat and element fluxes between the igneous crust and ocean water (Shipboard Scientific Party, 1997c). Upper Pliocene to Holocene sediment laps onto igneous basement within 20 km of the spreading axis of Juan de Fuca Ridge. Characterization of these strata becomes important if one's goal is to determine how the sediment cover influences the circulation and chemistry of hydrothermal fluids. As part of this characterization, we describe compositional data for turbidites and hemipelagic muds, interpret sediment provenance, and identify regional-scale pathways of sediment dispersal. By comparing interbeds of sand and mud, we also show whether or not the two types of sediment shared common detrital sources.

GEOLOGIC AND OCEANOGRAPHIC SETTING

Bathymetry

The surface area of Cascadia Basin is ~170,000 km², extending from the base of the Cascadia accretionary prism westward to the edge of sediment onlap onto juvenile basement of Juan de Fuca Ridge (Fig. 1). To the east, the muddy slope apron of the Cascadia subduction margin is underlain by deformed sequences of accreted abyssal

floor strata (Carson et al., 1974; Barnard, 1978; Davis and Hyndman, 1989; Hyndman et al., 1990). Near-shore bathymetry becomes more complicated toward the north because of Pleistocene glacial erosion. A large marine re-entrant (Strait of Juan de Fuca) connects inland waters of western Washington and British Columbia to the Pacific Ocean. The Strait of Georgia (Fig. 1), a steep and narrow passage between Vancouver Island and mainland British Columbia, merges into the eastern end of the Strait of Juan de Fuca. West of the Cascadia subduction front, the total thickness of deep-marine strata reaches a maximum of more than 3 km (Carlson and Nelson, 1987). The basin floor widens and slopes to the south. The average seafloor gradient is 1:1000, and the maximum water depth is 2930 m. The abyssal floor is highlighted by low-relief channel-levee complexes and two submarine fans (EEZ-SCAN 84 Scientific Staff, 1986).

Physical Oceanography

The water column above Cascadia Basin is affected by several currents that influence regional patterns of sediment dispersal. As the North Pacific Current approaches North America from the central Pacific, it splits into the north-flowing Alaskan Current (a counterclockwise gyre) and the south-directed California Current (e.g., Kirwan et al., 1978; Huyer, 1983; Lynn and Simpson, 1987; Shipboard Scientific Party, 1997d). The latitude of this separation migrates seasonally from ~50°N in summer to 43°N in winter and also drifts on decadal time scales. Generally, these surface currents are weak (4–8 cm/s). During winter, the Davidson Current also flows northward over the Oregon/Washington margin at 14–40 cm/s and merges with the eastern edge of the Alaska gyre. Less is known about bottom-water circulation within the region. A north-directed undercurrent moves at speeds up to 15 cm/s above the upper continental slope (Reid and Halpern, 1976; Halpern et al., 1978). Sluggish thermohaline currents in deeper water evidently transport suspended sediment toward the south (Stokke et al., 1977). A near-bottom nepheloid layer is well developed throughout the region; concentrations of suspended sediment are higher in submarine canyons (Baker, 1976; Stokke et al., 1977; Baker and Hickey, 1986).

¹Fisher, A., Davis, E.E., and Escutia, C. (Eds.), 2000. *Proc. ODP, Sci. Results*, 168: College Station TX (Ocean Drilling Program).

²Department of Geological Sciences, University of Missouri, Columbia MO 65211, USA. Correspondence author: UnderwoodM@missouri.edu

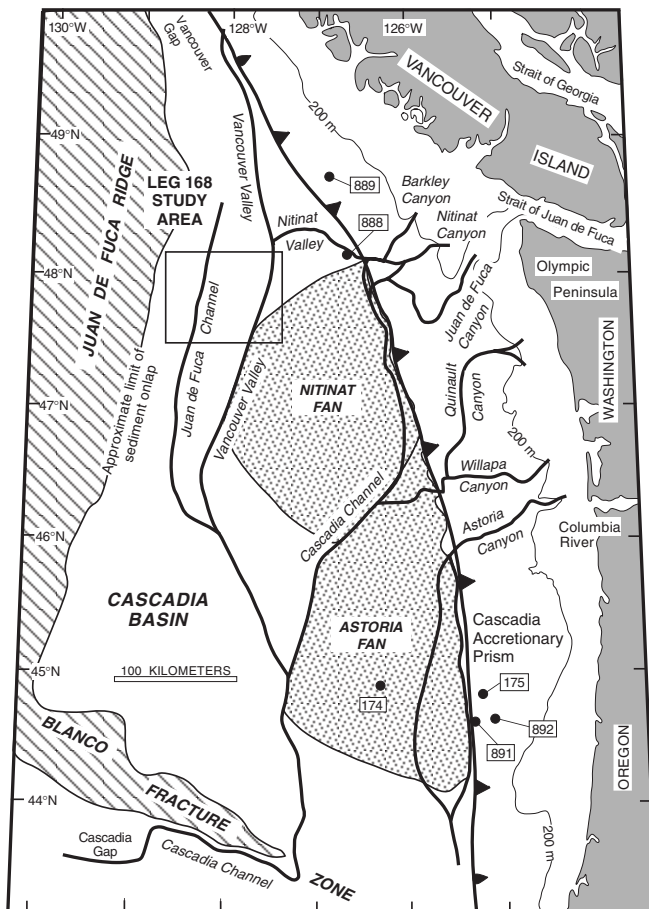


Figure 1. Physiography of the Cascadia Basin region (after Karl et al., 1989). Numbers in boxes refer to previous drill sites of the DSDP and ODP. Heavy line with teeth represents approximate position of the Cascadia subduction front and eastern edge of Cascadia Basin.

Depositional Character of Cascadia Basin

Average sedimentation rates on the Cascadia abyssal floor have been ~170 cm/k.y. during Pleistocene glacial intervals, whereas Holocene rates range from 2 to 10 cm/k.y. (Griggs et al., 1969). Submarine canyons function as the principal conduits for sediment transport onto the abyssal floor. Gravity-controlled processes (turbidity currents, debris flows, and slumps) have been more active during lowstands of sea level. During the Holocene highstand, canyons trap mostly fine-grained sediments and help focus sluggish downslope movement of the bottom nepheloid layer (Carlson and Nelson, 1969; Stokke et al., 1977; Baker and Hickey, 1986). The accretionary margin of southern Vancouver Island is incised by a long array of submarine canyons (Herzer, 1978; Davis and Hyndman, 1989). Another anastomosing network of canyons (Barkley, Nitinat, and Juan de Fuca) cuts the outer continental shelf near the termination of the Strait of Juan de Fuca (Fig. 1). Quinault Canyon begins on the outer continental shelf of Washington and hooks south across the middle forearc (Carson et al., 1986; Hickey et al., 1986; Thorbjarnarson et al., 1986). Farther south, Willapa and Astoria Canyons (Fig. 1) connect directly to the Columbia River mouth during lowstands of sea level (Carlson and Nelson, 1969; Baker, 1976; Barnard, 1978).

The floor of Cascadia Basin contains several important channel-levee complexes. Juan de Fuca Channel (Fig. 1), the westernmost example, originates in the northern portion of the basin (Carson, 1973). Vancouver Valley begins near 50°N, downslope of Vancouver Is-

land, and merges with Juan de Fuca Channel near 46°N. These two channels have created low-relief hummocks and swales near the Leg 168 transect area, and their maximum depth is about 70 m. Channels emanating from the mouth of the Barkley-Nitinat Canyon branch off to the west and south. Nitinat Valley intersects Vancouver Valley just north of the Leg 168 study area (Fig. 1). Cascadia Channel, the most prominent of the regional system, reaches a total length of over 2000 km (Griggs and Kulm, 1970). Beginning at the mouth of Juan de Fuca Canyon, this channel trends parallel to the base-of-slope toward its confluence with Willapa Channel (Karl et al., 1989). From there, it curves southwest between Nitinat and Astoria Fans, then turns south to join Vancouver Valley and several distributaries of Astoria Fan (Fig. 1). Cascadia Channel eventually intersects the Blanco Fracture Zone and passes west through Cascadia Gap onto the Tufts Abyssal Plain (Griggs and Kulm, 1970).

Nitinat Fan (Fig. 1), with an apex near the mouth of Barkley Canyon, is the most conspicuous depositional system of northern Cascadia Basin (Carson, 1973; Stokke et al., 1977). This elongate fan is bordered by Vancouver Valley to the west, Cascadia Channel to the east, and the fringes of Astoria Fan to the south. Astoria Fan (Fig. 1) radiates asymmetrically from the mouths of Astoria and Willapa Canyons. The Astoria system has prograded southward for more than 200 km between Cascadia Channel and the base-of-slope (Carlson and Nelson, 1969; Nelson et al., 1970; Nelson, 1976), but its influence on sedimentation within the Leg 168 study area, to the north, probably has been minimal.

Stratigraphy of Leg 168 Drilling Sites

Shipboard scientists during Leg 168 grouped ten drilling sites into three transects (Fig. 2). Sediment–basement relations range from outcrops of basalt near the spreading axis to deep burial by 600 m of sediment at Site 1027. With two exceptions (Sites 1030 and 1031), the stratigraphic successions include three lithostratigraphic units and display a crude upward-coarsening and upward-thickening trend (Fig. 3). Facies boundaries are time transgressive, so temporal correlations among sites have been made using nannofossil datums (Shipboard Scientific Party, 1997b, 1997e, 1997a; Su et al., Chap. 4, this volume). Within the context of our study, the designation of muds as “hemipelagic” refers to their texture (silty clay) and composition (mixture of biogenous and terrigenous constituents). Rigorous discrimination between the physical processes of deposition (i.e., muddy turbidity current vs. vertical settling) requires analysis of grain fabric by such methods as scanning electron microscopy (e.g., Giambalvo et al., in press). The hemipelagic deposits are typically structureless, with scattered clay-rich bands, silt laminae, zones of bioturbation, concentrations of calcareous nannofossils, and pyrite nodules. Subunit IA is composed of hemipelagic mud and coarser interbeds that range from medium-fine sand to sandy silt and silt. Most of the sand beds contain sedimentary structures that are diagnostic of turbidites: sharp to erosional bases, normal size grading, plane-parallel laminae, ripple cross-laminae, and wavy to convolute laminae. The deepest discrete sand layer defines the base of Subunit IA. Subunit IB contains thin interbeds of silt and hemipelagic mud, whereas Unit II is composed entirely of hemipelagic mud. The first recovery of basalt rubble defines the base of Unit II at each site.

The Hydrothermal Transition Transect includes Sites 1023, 1024, and 1025 (Fig. 2). This region, 20–35 km east of the Juan de Fuca Ridge, is characterized by a change from open-basement hydrothermal circulation to a sediment-covered basement. Basement ages inferred from magnetic anomalies range from 0.860 to 1.237 Ma. The wedge of sediment increases in thickness from 97 to 192 m toward the west above a relatively smooth basement surface (Fig. 3). Seismic reflection profiles also show small-scale levees between Sites 1025 and 1024 that are associated with the Juan de Fuca Channel (Shipboard Scientific Party, 1997b).

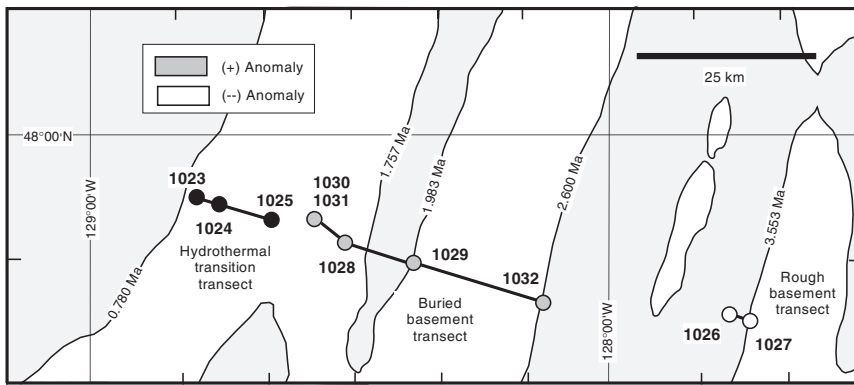


Figure 2. Magnetic-anomaly base map for the Leg 168 study area with locations of drill sites assigned to the Hydrothermal Transition, Buried Basement, and Rough Basement Transects (after Shipboard Scientific Party, 1997c). Positive anomalies are shaded, and ages of magnetic polarity transitions are given in Ma. See Figure 1 for regional context of study area.

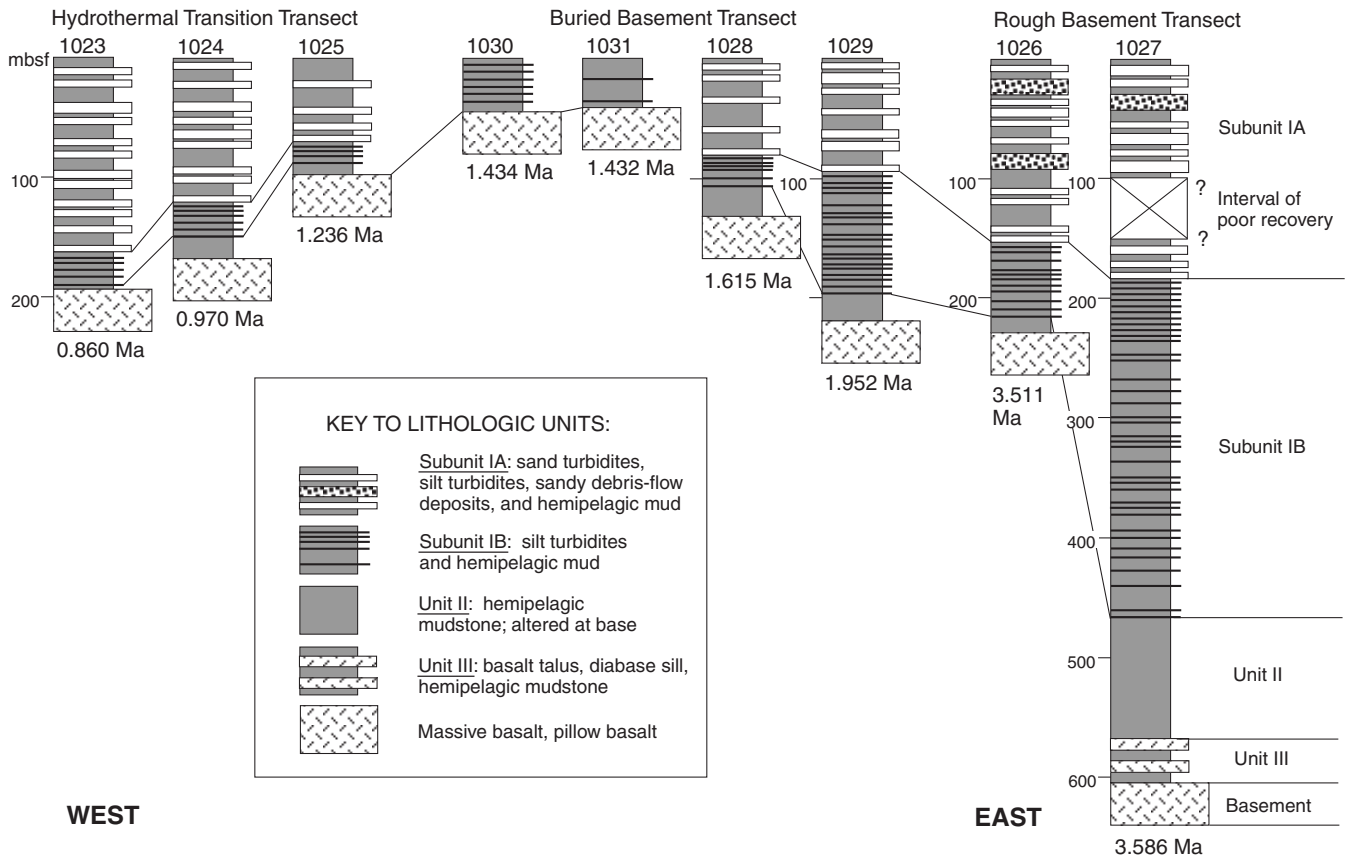


Figure 3. Lithostratigraphy of the Leg 168 drill sites. Ages of basaltic basement (from Shipboard Scientific Party, 1997c) are provided in Ma.

The Buried Basement Transect, 40–75 km east of the ridge axis, includes Sites 1028 through 1032 (Shipboard Scientific Party, 1997a). Basement ages range from 1.615 to 2.621 Ma (Fig. 2). For the most part, this region displays a relatively smooth basement surface and progressive eastward increases in sediment thickness. Sites 1030 and 1031, however, are situated directly above a basement high that rises to within 41.3 m of the seafloor (Fig. 3). Sediments from Sites 1030 and 1031 consist of hemipelagic mud, carbonate-rich mud, and rare beds of silt to sandy silt; these strata were not subdivided into lithostratigraphic units. Analyses of physical properties and fluid chemistry indicate that the sediments at Sites 1030 and 1031 are undercompacted and affected by upward flow of pore fluid (Shipboard Scientific Party, 1997a).

The Rough Basement Transect is located ~100 km east of the ridge axis (Fig. 2), in an area that contains linear basement ridges and

troughs (Shipboard Scientific Party, 1997e). Basement relief is typically 300–500 m, and some basement highs form seafloor outcrops. Site 1026 is located over a ridge, whereas Site 1027 is located above a basement valley (Fig. 3). Basement ages are 3.511 and 3.586 Ma, respectively (Fig. 2). Seismic reflection profiles near Site 1027 include a transparent interval roughly 0.2 s (two-way traveltimes) below the seafloor reflector; this interval corresponds to a zone of no core recovery (87–145 mbsf) and is probably composed of thick sand layers (Fig. 3). Recovered sand layers reach thicknesses up to 7 m. Two types of debris-flow deposits were also cored from this subunit; the first type is very poorly sorted muddy sand with a high proportion of primary matrix, and the second contains contorted mixtures of either muddy sand with mud clasts or clayey silt with mud clasts.

Depositional sites on the ridge flank have experienced substantial temporal changes in turbidite influx as dictated by thermal sub-

sidence of the lithosphere, tectonic and volcanic modification of basement structure, and the tendency of sediment-gravity flows to funnel between or deflect around bathymetric obstructions. The three-dimensional morphology of the seafloor changed dramatically over the past 3.5 m.y. as juvenile lithosphere subsided and moved away from the spreading ridge and basement lows filled with sediment. Gradual smoothing out of the seafloor, in turn, affected the behavior of unconfined sheet flows and channel-levee complexes. This dynamic link between sedimentation and geomorphology helps account for the large spatial and temporal differences in total accumulation rates and turbidite recurrence intervals (Shipboard Scientific Party, 1997b, 1997e, 1997a).

Deposition at Site 1027 began soon after basement formed at 3.586 Ma. Initially, this valley filled slowly by suspension fallout, but as basement obstructions to the east were buried, the first silty turbidity currents encroached at ~1.6 Ma. By 1.1 Ma, sandy sediments had filled the valley and turbidites began to lap onto the nearby ridge beneath Site 1026. Farther west, the basement high beneath Sites 1030 and 1031 continued to block transport of turbidity currents to the Hydrothermal Transition sites until ~0.45 Ma (Shipboard Scientific Party, 1997b). The most recent episode of sedimentation (<90 ka) has included westward progradation of channel-levee deposits within the Hydrothermal Transition Transect area.

LABORATORY METHODS

Samples for sand petrography were immersed in 3% H₂O₂ solution for at least 24 hr to remove organic material. Sodium hexametaphosphate solution (4 g/1000 mL) was added to disaggregate and disperse clays. Suspensions were placed on a magnetic stirrer, then wet sieved with a 63- μ m screen. The fine fractions were saved for X-ray diffraction analysis. After drying the coarse fraction, standard thin sections were prepared from epoxy grain mounts, and plagioclase and potassium feldspars were stained following Houghton (1980). We used the Gazzi-Dickinson point-counting method, whereby all sand-sized minerals are assigned to their respective mineral categories, even if they occur in polycrystalline rock fragments (Dickinson, 1970). A sand-sized plagioclase phenocryst in a volcanic-rock fragment, for example, counts as plagioclase rather than the host lithic grain. Ingersoll et al. (1984) demonstrated that this approach significantly reduces the sensitivity of compositional data to grain size. Step sizes for point counts were 0.4 mm between tracks and 0.6 mm along tracks. At least 500 grains were counted per thin section. Grain types were assigned to 22 categories, then combined into conventional monocrystalline and polycrystalline modes (Table 1). Replicate analyses showed that the average standard deviations for these detrital modes (in percent) are: Q = 4, F = 4, and L = 3; Q_m = 3, F = 4, and L_i = 3; Q_v = 5, P = 5; and K = 2; and Q_p = 5, L_v = 6, and L_{sm} = 5 (Saettler, 1998).

Samples of turbidite matrix and hemipelagic mud were prepared for X-ray diffraction analysis using the same techniques. After sieving, all <63- μ m suspensions were disaggregated further using an ultrasonic cell probe, then centrifuged at 1000 rpm for 2.4 min to separate the <2- μ m fraction. Oriented aggregates of the <2- μ m fraction were collected on vacuum filters, peeled onto glass slides, and saturated with ethylene glycol vapor for at least 12 hr at 60°C before scanning. We used a Scintag Pad V X-ray diffractometer, with CuK α radiation (1.54 Å) and a Ni filter. Scans were run at 40 kV and 30 Ma from 3 to 19°2 θ at a rate of 2°2 θ /min and a step size of 0.01°2 θ . Processing of digital data utilized MacDiff software to smooth counts, determine background levels, and calculate peak intensities and peak areas. To help facilitate comparisons with existing data from the region (e.g., Karlin, 1980), the integrated areas of smectite (001), illite (001), and chlorite (002) peaks were multiplied by Biscaye (1965) weighting factors (1 \times , 4 \times , and 2 \times , respectively), then normalized to 100%. Chlorite content was calculated using the peak near 12.5°2 θ

(d-value = 7.10 Å), but peak interference can be problematic if there is a strong kaolinite (001) reflection (d-value = 7.16 Å). Consequently, nine samples were tested for kaolinite content by boiling in 1-N HCl for 2 hr (Biscaye, 1964). The kaolinite contribution proved to be less than 7% of the composite peak area, with an average of 5% (Saettler, 1998). Three types of error in the precision of mineral percentages were tested by replicate analysis: natural inhomogeneity of subsamples (<4%), diffractometer instability (<2%), and inconsistent manipulation of data-processing software (<1%). Accuracy of the Biscaye (1965) weighting factors, however, also varies with the absolute abundance of each mineral (e.g., Underwood et al., 1993). Moore and Reynolds (1997) concluded that accuracy is generally no better than 10% for major constituents. Our data, therefore, should be regarded as semiquantitative estimates and used to compare relative trends in mineralogy rather than as absolute abundance.

RESULTS

Sand Petrography

Point counting was used to analyze 134 thin sections. Statistical comparisons among sites are shown in Table 2. Table 3 contains complete point-count data, and Table 4 lists all detrital modes. In general, fluctuations of detrital modes are within the limits of point-counting precision. The modal values of total quartz, total feldspar, and lithic fragments (Q-F-L) are approximately equal in most samples (Figs. 4–6). The largest variations generally occur within the polycrystalline constituents (Q_p-L_v-L_{sm}), but some of this scatter may be a statistical artifact of small subset populations.

One of the more interesting discoveries from the Hydrothermal Transition Transect is that sandy silt layers from the lower part of Subunit IA and from Subunit IB contain over 70% (typically over 90%) of what we interpret to be intraformational mud chips. One sample from Site 1028, immediately above the 0.28-Ma datum, also contains abundant intrabasinal mudstone clasts. The mudstone particles are typically brownish yellow in color and contain silt-sized grains of monocrystalline quartz, plagioclase, calcite, microfossils, opaque grains, mica, and mafic minerals in a clay matrix. These clasts of cohesive sediment probably were remobilized off adjacent basement highs.

Temporal variations in sand composition within and among the Leg 168 sites are not pronounced. Except for the lithic-rich intraformational deposits, sand composition within the Hydrothermal Transition Transect is quite homogeneous (Fig. 4). Sand samples from Sites 1028 and 1029 are also fairly homogeneous in Q-F-L modes; variations in polycrystalline constituents are larger and more erratic (Fig. 5). Systematic temporal changes in sand composition occur only within the Rough Basement Transect. Polycrystalline quartz and

Table 1. Categories of detrital grains included in petrographic point counts of turbidite sand.

Categories of detrital grains
Modal constituents:
Q = total quartz = Q _m + Q _p
Q _m = monocrystalline quartz
Q _p = polycrystalline quartz = microcrystalline + cryptocrystalline
F = total feldspar = P + K
P = plagioclase
K = K-feldspar = orthoclase + perthite
L = unstable lithic fragments = L _v + L _v + L _{sm}
L _v = sedimentary = claystone + mudstone + siltstone
L _v = volcanic = mafic (basaltic) + intermediate (andesitic) + silicic (rhyolitic)
L _{sm} = metamorphic = quartz-mica tectonite + slate-phyllite
L _{sm} = sedimentary + metasedimentary
L _i = total polycrystalline fragments = L + Q _p
Accessory constituents:
Heavy minerals = opaque + non-opaque
Mica = muscovite + biotite
Biogenic = fossil fragments + sparry calcite
Other = trace constituents + altered grains + unknown

Table 2. Statistical summary of detrital sand modes and clay mineralogy, Cascadia Basin.

	All constituents Q-F-L modes*			All constituents Q _m -F-L _i modes			Monocrystalline Q _m -P-K modes			Polycrystalline Q _p -L _v -L _{sm} modes			Polycrystalline L _v -L _s -L _m modes			Clay mineralogy			
	Q	F	L	Q _m	F	L _i	Q _m	P	K	Q _p	L _v	L _{sm}	L _v	L _s	L _m	Smec	Illite	Chl + Kaol	
Hydrothermal Transition Transect																			
Site 1023:																			
Average [†]	37	34	29	30	34	36	47	48	5	19	38	43	47	42	11	7	42	51	
SD [†]	3	2	3	3	2	4	3	3	2	5	6	6	7	7	3	68	7		
Maximum [†]	45	38	34	37	38	42	53	53	10	27	48	55	61	53	16	22	59	67	
Minimum [†]	33	29	22	26	29	30	41	42	0	9	27	28	35	31	5	1	26	36	
Site 1024:																			
Average [†]	37	34	29	31	34	35	47	49	4	16	41	43	49	44	7	11	38	51	
SD [†]	3	3	3	3	3	4	3	3	2	4	8	9	10	11	3	9	7	7	
Maximum [†]	41	40	34	35	40	41	53	53	10	23	54	62	66	65	11	31	50	62	
Minimum [†]	30	30	23	26	30	26	42	41	1	11	27	28	30	30	3	1	29	38	
Site 1025:																			
Average [†]	34	34	32	29	33	38	46	49	5	16	39	45	47	42	11	10	40	50	
SD [†]	2	4	4	2	4	5	3	3	3	4	7	7	8	7	5	8	8	10	
Maximum [†]	40	42	40	33	42	46	50	54	10	22	53	57	57	56	22	31	51	70	
Minimum [†]	30	27	25	25	27	30	40	43	2	8	28	34	36	35	5	0	25	32	
Buried Basement Transect																			
Site 1028:																			
Average	31	33	36	28	33	39	46	48	6	10	41	49	46	47	7	8	40	52	
SD	7	7	13	6	7	13	4	4	3	5	15	19	18	20	3	8	8	9	
Maximum	40	45	71	36	45	73	52	55	9	18	57	97	70	99	12	34	51	69	
Minimum	13	15	23	12	15	26	39	42	2	2	1	25	1	21	0	2	25	41	
Site 1029:																			
Average	33	35	32	27	35	38	44	51	5	15	45	40	53	38	9	7	43	50	
SD	4	4	5	5	4	5	6	5	2	7	10	11	11	12	5	6	6	7	
Maximum	41	44	44	36	44	47	50	63	10	31	59	59	73	61	18	20	53	63	
Minimum	24	29	22	19	29	28	34	44	2	5	32	22	36	19	1	1	34	30	
Site 1030:																			
Average	No sand analyzed																		
SD																5	45	50	
Maximum																	5	8	8
Minimum																	15	60	64
Site 1031:																			
Average	No sand analyzed																		
SD																3	48	49	
Maximum																	3	8	8
Minimum																	11	65	62
Rough Basement Transect																			
Site 1026:																			
Average	35	38	27	30	38	32	44	50	6	17	46	37	55	34	11	7	43	50	
SD	5	4	4	5	4	4	6	5	3	6	9	10	11	11	4	6	7	7	
Maximum	45	46	36	38	46	41	57	61	13	29	60	76	71	75	21	25	57	63	
Minimum	28	30	21	20	30	25	33	41	1	5	19	24	20	21	5	0	32	38	
Site 1027:																			
Average	34	37	29	28	37	35	43	51	6	16	51	33	61	30	9	6	39	55	
SD	4	4	4	4	4	6	5	5	3	5	7	9	9	10	4	7	8	8	
Maximum	40	51	38	33	51	47	50	65	14	29	67	50	85	50	19	38	49	78	
Minimum	26	31	22	19	31	26	30	43	1	8	38	12	44	9	3	1	19	39	

Note: * = see Table 1 for explanation of abbreviations, † = excludes intraformational deposits, SD = standard deviation. Smec = smectite, Chl + Kaol = chlorite + kaolinite.

Table 3. Petrographic point-count data, turbidite sand deposits, Cascadia Basin.

Core, section, interval (cm)	Depth (mbsf)	Quartz		Feldspar		Lithic fragments			Accessory constituents				Total points counted	
		Monocrystal	Polycrystal	Plagioclase	K-spar	Sediment	Metamorphic	Volcanic	Heavy mineral	Mica	Biogenic	Other		
168-1023A-														
1H-6, 54	8.04	161	14	149	19	49	14	72	18	0	14	7	517	
3H-6, 55	26.87	116	14	123	7	56	17	45	25	18	40	50	511	
4H-7, 34	37.64	138	37	127	19	47	24	81	27	1	12	15	506	
5H-1, 50	38.30	138	16	140	12	51	18	62	30	9	17	14	507	
5H-6, 126	46.56	127	33	128	12	67	18	56	15	12	21	12	512	
6H-2, 47	49.27	131	38	116	10	73	8	67	28	6	35	13	521	
7H-3, 61	60.41	137	44	135	13	70	16	47	20	9	27	6	518	
7H-5, 101	63.81	132	37	128	14	47	11	56	37	8	16	5	496	
8H-1, 78	67.08	129	40	140	0	62	19	59	25	2	18	13	510	
8H-2, 26	68.06	163	27	144	6	50	9	77	23	7	19	19	510	

This is a sample of the table that appears on the volume CD-ROM.

Table 4. Detrital models for turbidite sand deposits, Cascadia Basin.

Core, section, interval (cm)	Depth (mbsf)	Q-F-L modes			Q _m -F-L _i modes			Q _m -P-K modes monocrystalline			Q _v -L _v -L _{sm} modes polycrystalline			L _v -L _v -L _{sm} modes unstable lithic		
		Total quartz	Total feldspar	Unstable lithic	Mono quartz	Total feldspar	Total lithic	Qtz	Plag	Kspr	Qtz	Vol	S+M	Vol	Sed	Meta
168-1023A-																
1H-6, 54	8.04	37	35	28	34	35	31	49	45	6	9	48	42	53	36	10
3H-6, 55	26.87	34	34	31	31	34	35	47	50	3	11	34	55	38	47	14
4H-7, 34	37.64	34	32	34	26	32	42	44	48	7	20	43	38	53	31	16
5H-1, 50	38.30	35	35	30	32	35	38	48	48	4	11	42	47	47	39	14
5H-6, 126	46.56	38	31	31	31	31	42	50	46	4	19	32	49	40	48	13
6H-2, 47	49.27	38	29	34	29	29	39	50	46	4	20	36	44	45	49	5
7H-3, 61	60.41	38	32	29	29	32	35	47	48	5	25	27	49	35	53	12
7H-5, 101	63.81	40	33	27	32	33	40	49	46	5	25	37	38	49	41	10
8H-1, 78	67.08	38	31	31	29	31	37	49	51	0	22	33	45	42	44	14
8H-2, 26	68.06	35	34	31	29	34	31	46	52	2	17	47	36	57	37	7

This is a sample of the table that appears on the volume CD-ROM.

volcanic-rock fragments at Site 1026 (above basement high) increase steadily above the 0.28-Ma datum, whereas sedimentary-rock plus metamorphic-rock fragments decrease upsection from 75% to 27% (Fig. 6). These trends, however, are not apparent at Site 1027 (above adjacent basement low). Above the 0.09-Ma datum, Sites 1026 and 1027 show consistent increases in sedimentary-rock plus metamorphic-rock fragments (Fig. 6).

Clay Mineralogy

Clay mineral abundance was determined from 130 samples of mud (both hemipelagic and turbidite) and 47 samples of matrix clay from sand and silt turbidites. Values of peak intensity (counts), integrated peak area (total counts), and peak width at half height ($\Delta^{\circ}2\theta$) are listed in Table 5. Relative clay mineral abundance are listed in Table 6. In general, fluctuations in mineral abundance are erratic with depth and age; contrasts among lithostratigraphic units and sites are subtle.

Smectite content is consistently low in all of the samples analyzed (Table 2). At Site 1023, for example, values for hemipelagic mud samples range between 2% and 20% (Fig. 7). Values range from 3% to 20% within Subunit IA, from 2% to 16% within Subunit IB, and from 2% to 5% within Unit II. Similar results were obtained for samples from Sites 1024 and Site 1025 (Table 2). At Site 1028, Subunit IA contains 5%–35% smectite (Fig. 7), whereas values in Unit II increase from 5% to 20%. Smectite abundance at Site 1029 also increases in Unit II and upsection within Subunit IA. Relative abundance at Site 1026 (Rough Basement Transect) are 4%–16% in Subunit IA, 2%–13% in Subunit IB, and 0%–25% within Unit II (Fig. 7). Mud samples from Site 1027 contain less than 12% smectite throughout the section.

The relative abundance of illite in mud deposits at the Hydrothermal Transition sites ranges from 30% to 50%, and chlorite + kaolinite ranges from 40% to 75%. Similar scatter occurs across the Rough Basement and Buried Basement Transects (Fig. 7). At Site 1026, for example, illite abundance is 32%–57%, changing very little among stratigraphic units, whereas chlorite + kaolinite varies between 38% and 63%. At Site 1027, mud samples contain 19%–49% illite (increasing upsection) and 39%–78% chlorite + kaolinite (decreasing upsection).

The relatively thin accumulations of hemipelagic mud at Sites 1030 and 1031 are situated above a basement high; these strata are intriguing because their grain fabrics have not compacted and their pore-fluid compositions are consistent with fluid upflow (Shipboard Scientific Party, 1997a). Our results show that the clay minerals in these muds are not unusual (Fig. 7). When compared to the other sites, samples from Sites 1030 and 1031 contain slightly less smectite (mean values of 5% and 3%), slightly more illite (mean values of 45% and 48%), and similar amounts of chlorite + kaolinite (mean

values of 50% and 49%). These subtle compositional shifts are probably not enough to account for the documented differences in compaction behavior (Giambalvo et al., in press).

We also analyzed the <2- μ m-size fractions from coarse turbidites to determine whether or not their relative mineral abundance change systematically with respect to those of silty clay interbeds (Tables 5, 6). Differences in clay mineralogy are <10% in more than half of the sample pairs analyzed, but shifts >20% also occur (Fig. 8). As an extreme example, the highest content of smectite from our study (38%) occurs within a turbidite sand at Site 1027, whereas the overlying mud contains only 12% smectite. None of the mineral groups, however, exhibits a consistent sense of change from one lithology to the other, so we cannot attribute differences in clay composition solely to the effects of selective partitioning by grain size or depositional process.

DISCUSSION

Sediment Sources

Sand Provenance

Siliciclastic detritus recovered during Leg 168 was eroded from igneous, metamorphic, sedimentary, and metasedimentary rocks. With the exception of the sand layers with abundant intraformational mud clasts, the turbidite samples are remarkably consistent in composition (Table 2). Figure 9 shows that mean values for total-grain modes ($Q = 35$, $F = 35$, $L = 30$) plot within the generic dissected-arc provenance field, as defined by Dickinson et al. (1983). Q_m -P-K data (mean of $Q_m = 46$, $P = 49$, and $K = 5$) plot within the Circum-Pacific volcano-plutonic suite of Dickinson (1982). Polycrystalline modes agree with the arc-orogen field of Dickinson and Suczek (1979), with a mean of $Q_p = 16$, $L_v = 43$, and $L_{sm} = 41$. The mean values of $L_v = 52$, $L_s = 39$, and $L_m = 9$ are consistent with a mixed magmatic-arc and rifted-continent source (Fig. 9).

Several specific sources and fluvial systems need to be considered in our interpretation of provenance. The Queen Charlotte Islands and Vancouver Island, for example, contain Cambrian to Tertiary volcanic, sedimentary, and granitic rocks (Muller, 1977; Clague, 1986). Common lithologies on southern Vancouver Island include metasedimentary and igneous rocks overlain by submarine volcanic rocks of Eocene age. The Coast Plutonic Complex of western British Columbia, Washington, and northern Oregon consists mainly of Cretaceous granitic intrusions, Jurassic to Tertiary sedimentary and volcanic rocks in the south, and Precambrian to Tertiary sedimentary and volcanic rocks in the north (Clague, 1986). The uplifted core of the Olympic Peninsula consists mostly of Tertiary metasedimentary rocks, surrounded by basalt of the Crescent Volcanics (Tabor and Cady, 1978; Brandon et al., 1998); sedimentary deposits are widespread along the west and north coasts of the peninsula. Farther east,

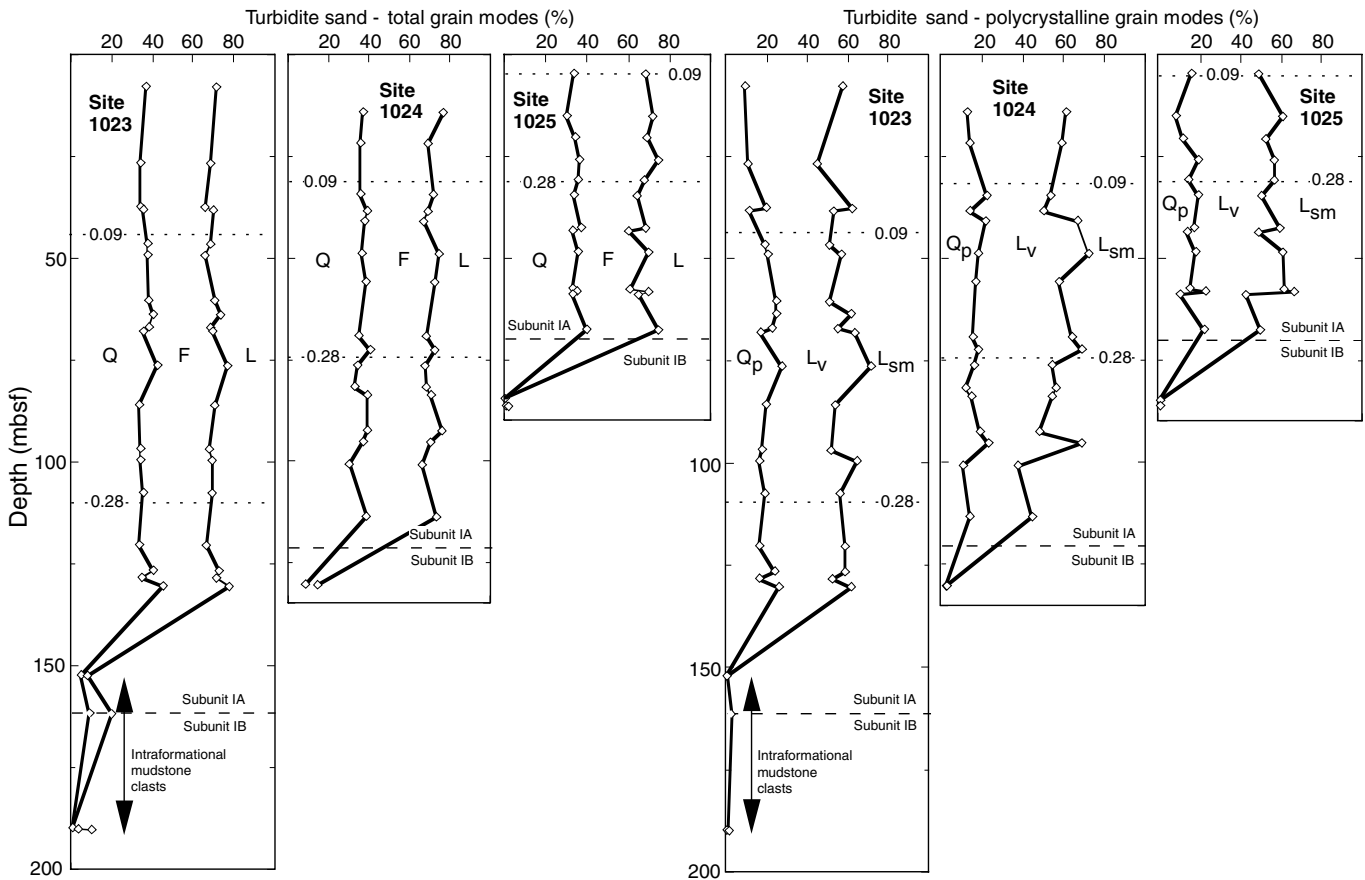


Figure 4. Area plots showing depth variations in detrital modes for turbidite sands from Sites 1023, 1024, and 1025 (Hydrothermal Transition Transect). Numbers refer to ages (in Ma) of nanofossil datums (from Su et al., Chap. 4, this volume). Q = total quartz; F = total feldspar; L = unstable lithic fragments; Q_p = polycrystalline quartz; L_v = volcanic-rock fragments; and L_{sm} = sedimentary-rock and metasedimentary-rock fragments.

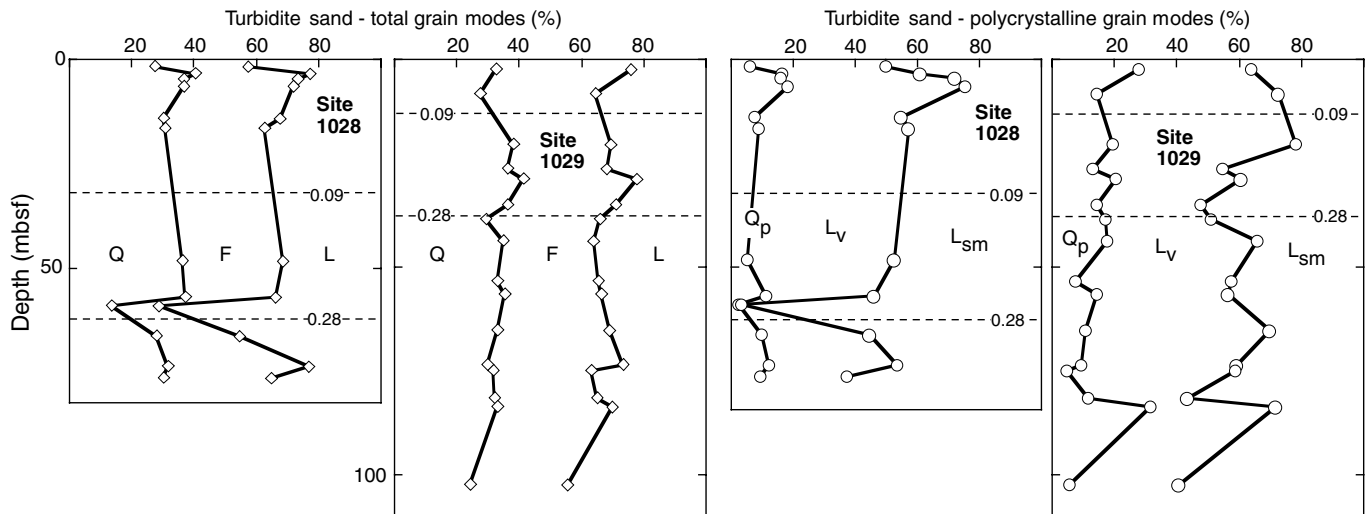


Figure 5. Area plots showing depth variations in detrital modes for turbidite sands from Sites 1028 and 1029 (Buried Basement Transect). Numbers refer to ages (in Ma) of nanofossil datums (from Su et al., Chap. 4, this volume). Abbreviations are as explained in Figure 4.

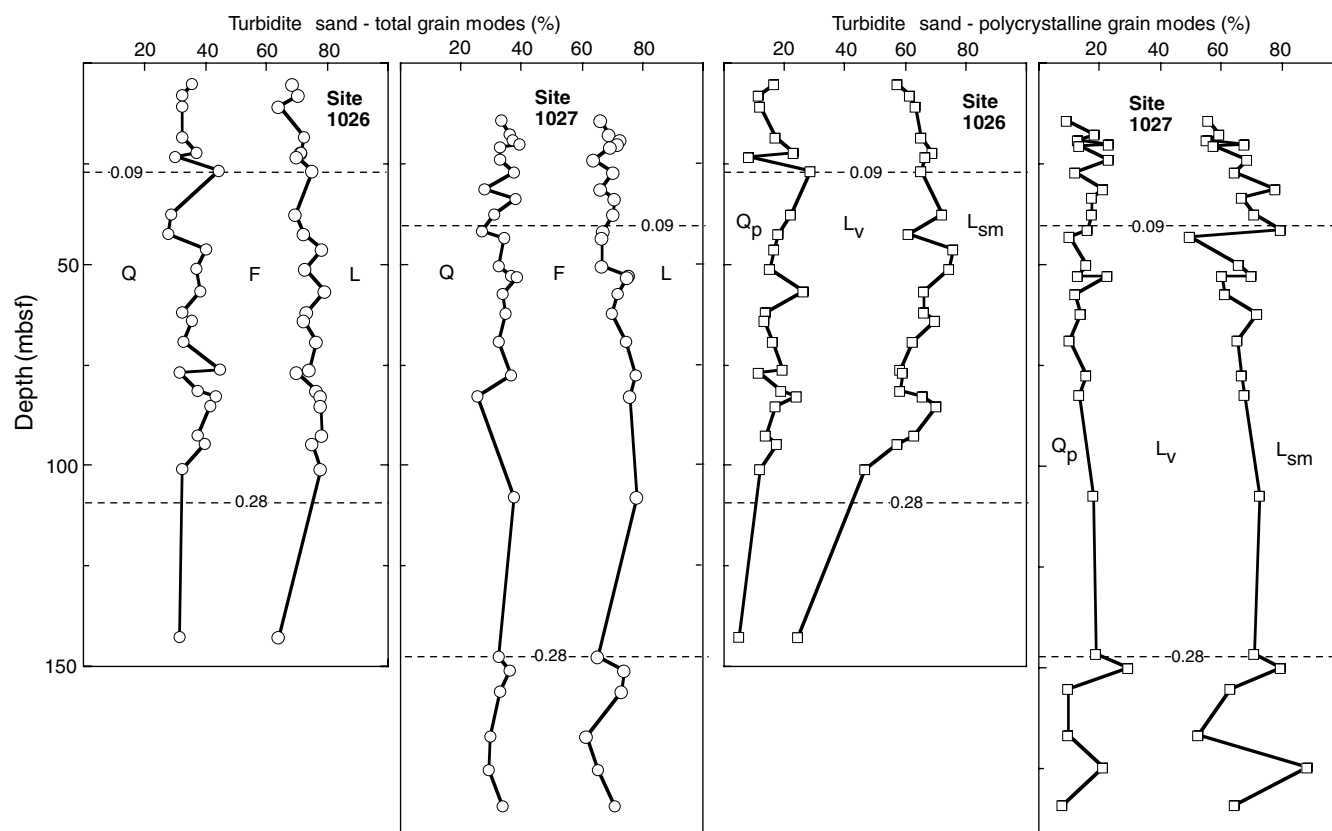


Figure 6. Area plots showing depth variations in detrital modes for turbidite sands from Sites 1026 and 1027 (Rough Basement Transect). Numbers refer to ages (in Ma) of nanofossil datums (from Su et al., Chap. 4, this volume). Abbreviations are as explained in Figure 4.

Table 5. Results of X-ray diffraction analyses, hemipelagic mud, and turbidite matrix, <2- μ m-size fraction, Cascadia Basin.

Core, section, interval (cm)	Depth (mbsf)	Stratigraphic unit	Lithology	Smectite (001) peak			Illite (001) peak			Chlorite (001) peak		
				Area (total cts)	Intensity (cts/s)	Width FWHM ($^{\circ}2\theta$)	Area (total cts)	Intensity (cts/s)	Width FWHM ($^{\circ}2\theta$)	Area (total cts)	Intensity (cts/s)	Width FWHM ($^{\circ}2\theta$)
168-1023A-												
1H-6, 54-61	8.04	IA	T	8754	96	0.876	4309	133	0.227	7157	206	0.253
1H-6, 78-84	8.28	IA	M	2681	35	0.998	1448	39	0.240	4051	88	0.323
3H-3, 108-112	22.90	IA	M	285	8	0.195	1205	33	0.197	2323	91	0.170
3H-3, 125-129	23.07	IA	T	380	11	0.280	1359	41	0.162	3493	130	0.154
4H-3, 21-23	31.51	IA	T	130	5	0.000	997	24	0.223	1602	55	0.190
4H-3, 26-28	31.56	IA	M	281	10	0.298	1974	66	0.167	3044	137	0.160
5H-1, 50-55	38.30	IA	T	84	7	0.000	2026	70	0.188	2824	106	0.182
5H-1, 59-64	38.39	IA	M	1131	21	0.562	1450	45	0.237	2551	83	0.217
9H-1, 60-65	76.40	IA	T	3450	41	0.869	2219	64	0.230	6797	197	0.230
9H-1, 72-77	76.52	IA	M	4816	56	1.075	3310	68	0.331	9006	241	0.254

Note: T = matrix from turbidite sand/silt, M = hemipelagic mud.

This is a sample of the table that appears on the volume CD-ROM.

the crystalline core of the Cascade Range is made up of Devonian to middle Tertiary metamorphic-plutonic complexes (Blakely and Jachens, 1990). The Western Cascades consist of basaltic, andesitic, and dacitic lava flows intercalated with pyroclastic rocks. Quaternary volcanic complexes of the High Cascades are basaltic to rhyolitic in composition, with andesite the most common lithology (McBirney, 1978). Collectively, mechanical weathering of these source regions should produce a diverse mixture of sand-sized grain types.

Differences in sample preparation and counting technique preclude reliable statistical comparisons among data sets, but several previous studies provide qualitative insights into the regional patterns of sediment dispersal. The Columbia River (Fig. 1) is the largest point source of fluvial discharge to Cascadia Basin, with headwaters

extending eastward into the Rocky Mountains (Whetten et al., 1969). The upper Columbia sub-basin is underlain by sedimentary strata, plutonic, and coarse metamorphic bedrock (Knebel et al., 1968); widespread flood basalts contribute volcanic-lithic grains to the middle and lower basin (Beeson and Tolan, 1990), whereas andesitic debris from the High Cascades increases toward the river mouth (Whetten et al., 1969). Unfortunately, characterization of the Columbia River system in its natural state has been compromised by construction of numerous dams and reservoirs. Deposits in the westernmost reservoir (Bonneville) yield average Q-F-L values of Q = 32, F = 32, and L = 38, whereas samples between Bonneville reservoir and the river mouth average Q = 14, F = 28, and L = 58 (Whetten et al., 1969). Offshore, White (1970) showed that Holocene sands on the

Table 6. Relative abundance of clay minerals, <2- μ m-size fraction, Cascadia Basin.

Core, section, interval	Depth (mbsf)	Stratigraphic unit	Lithology	Relative abundance clay mineral		
				Smectite (%)	Illite (%)	Chlorite + Kaolinite (%)
168-1023A-						
1H-6, 54-61	8.04	IA	T	22	43	36
1H-6, 78-84	8.28	IA	M	16	35	49
3H-3, 108-112	22.90	IA	M	3	49	48
3H-3, 125-129	23.07	IA	T	3	42	55
4H-3, 21-23	31.51	IA	T	2	54	44
4H-3, 26-28	31.56	IA	M	2	55	43
5H-1, 50-55	38.30	IA	T	1	59	41
5H-1, 59-64	38.39	IA	M	9	48	42
9H-1, 60-65	76.40	IA	T	13	34	52
9H-1, 72-77	76.52	IA	M	13	37	50

Note: T = turbidite matrix, H = hemipelagic mud.

This is a sample of the table that appears on the volume CD-ROM.

Washington-Oregon shelf are also enriched in lithic fragments. Average modes for the shelf deposits are $Q = 16$, $F = 22$, and $L = 62$, in reasonable agreement with the lower reaches of the Columbia River.

Farther north, the Fraser River empties into the Strait of Georgia (Fig. 1) near the city of Vancouver; this fluvial system drains over 250,000 km² of geologically diverse terrain in south-central British Columbia (Pharo and Barnes, 1976; Clague et al., 1983). Garrison et al. (1969) showed that lithic grains and detrital quartz dominate the sand fraction of the Fraser River delta; average Q-F-L modes are $Q = 42$, $F = 11$, and $L = 47$. Discharge from the Fraser River mixes down-current with smaller streams that drain both southern Vancouver Island and the Olympic Peninsula (Mayers and Bennett, 1973). Collectively, this system creates a second major point source emanating from the Strait of Juan de Fuca, with sediments reflecting a mixture of many tributary sources and rock types.

Working offshore, Carson (1971) concluded that Holocene and Pleistocene near-surface sands in northwestern Cascadia Basin (including the northern part of Vancouver Valley) came from the west coast of Vancouver Island, and that influx from southern Vancouver Island and the Olympic Peninsula becomes increasingly important farther to the south. Chamov and Murdmaa (1995) studied samples from the northern edge of Nitinat Fan (ODP Site 888) and the Vancouver accretionary prism (ODP Site 889). Their average Q-F-L values for light-density grains (segregated using heavy liquids) are $Q = 46$, $F = 18$, and $L = 36$ (Site 888) and $Q = 41$, $F = 19$, and $L = 40$ (Site 889). These modes are similar to those documented at the Fraser River mouth (Garrison et al., 1969). Farther south, Scheiddeger et al. (1973) recognized two petrofacies of heavy minerals at Deep Sea Drilling Project (DSDP) Site 174 (Fig. 1). An amphibole-rich petrofacies (Pliocene) was derived from either the Klamath Mountains of southern Oregon or Vancouver Island, whereas the overlying Quaternary deposits match a Columbia River source. Near-surface sands from southern Cascadia Basin also contain lithic-rich light-mineral suites that probably were transported from the Columbia River (Duncan and Kulm, 1970).

Our results compare most favorably with the data of Gergen and Ingersoll (1986) and Marsaglia and Ingersoll (1992), who analyzed sands from DSDP sites using similar techniques. Sands from DSDP Site 177, which is located well to the north of our study area (50°28'N), contain much higher percentages of feldspar ($Q = 29$, $F = 58$, and $L = 13$) and more sedimentary-rock and metamorphic-rock fragments ($L_v = 25$, $L_s = 48$, and $L_m = 27$) as compared to the samples from Leg 168 (Fig. 9). Based largely on these negative comparisons, we conclude that the flux of sand into the Leg 168 corridor from detrital sources north of Vancouver Island was not significant. The average detrital modes for Quaternary sands at DSDP Site 174 (distal Astoria Fan) are $Q = 36$, $F = 40$, and $L = 24$; proportions of volcanic-rock to sedimentary + metamorphic-rock fragments are roughly

equal, and monocristalline modes are $Q_m = 46$, $P = 40$, and $K = 14$ (Fig. 9). This petrofacies typifies Columbia River output during the Quaternary and comes fairly close to matching the modal character of Leg 168 samples (Fig. 9). The Pliocene abyssal-plain facies beneath Astoria Fan shows an interesting shift to more lithic-rich composition ($Q = 21$, $F = 27$, and $L = 52$), with a significant increase in volcanic-rock fragments ($L_v = 69$, $L_s = 6$, and $L_m = 25$). Although a Vancouver Island provenance was suggested for the Pliocene lithofacies by Scheiddeger et al. (1973), its petrographic character differs significantly from our Leg 168 results. We believe that additional criteria are required to discriminate more effectively between potential point sources at the mouths of the Columbia River and Strait of Juan de Fuca.

Clay Provenance

Under circumstances typical of siliciclastic margins, interbeds of turbidite sand and hemipelagic mud usually share common detrital sources (e.g., Underwood et al., 1993), but this expectation is not always realized. Transport directions can be different for downslope-seeking density currents, surface-water plumes, and (or) isobath-parallel bottom currents (Underwood, 1986; Hathon and Underwood, 1991). Selective partitioning of size fractions by transporting agents can also cause contrasts in mineral abundance and clay crystallinity (Gibbs, 1977; Carson and Acaro, 1983). Sluggish nepheloid-layer transport down submarine canyons might be particularly susceptible to size partitioning (Baker, 1976). Smectite tends to increase in the smaller size fractions, and chlorite tends to increase in coarser size fractions. Thus, one might expect grain-size partitioning to reduce smectite in turbidite sands relative to muddy interbeds.

In our study, relative abundance of clay minerals within adjacent sand/mud pairs are similar enough to argue for a shared detrital source. More significantly, we did not document any systematic shifts in clay mineralogy in consort with the type of host lithology. Some of the erratic variations probably represent the natural heterogeneity of the clay-sized sediment budget. Another contributing factor might be intermingling of nepheloid clouds, mass flows, and surface currents converging on the study area from several directions. Finally, glacial-interglacial climate change during the Pleistocene probably played a role in the zonation of weathering behavior; the resolution of our nannofossil age control is not high enough, however, to define or recognize such climate-driven cycles in the depositional record.

As with our petrographic data, quantitative comparisons with and among previously published data sets are inhibited by differences among the sample types, methods of sample preparation, and X-ray diffraction systems. As one qualitative comparison, Holocene clay-mineral suites from the lowermost reservoir of the Columbia River

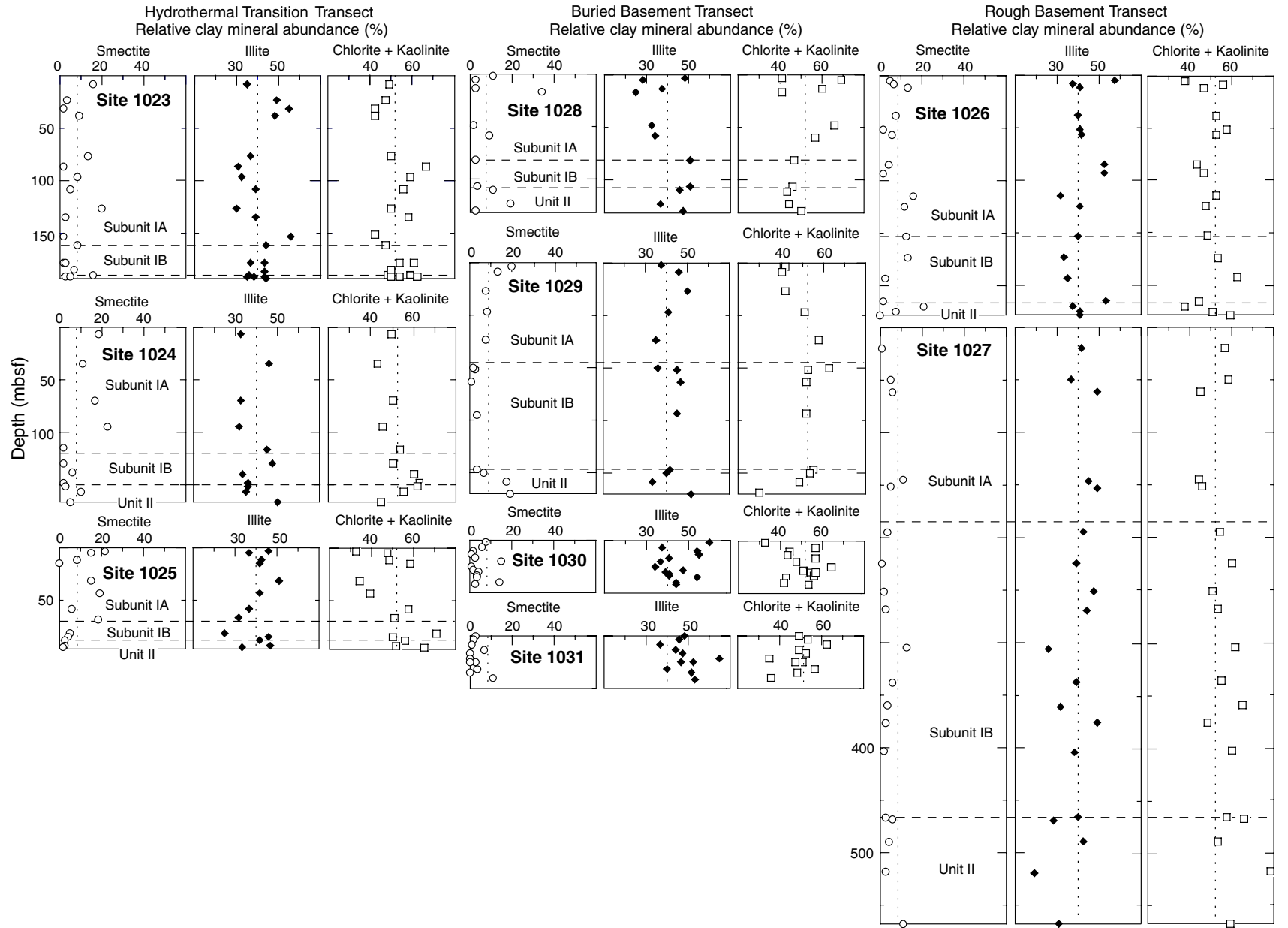


Figure 7. Depth variations in relative abundance of smectite, illite, and chlorite + kaolinite (<math><2\text{-}\mu\text{m}</math>-size fraction) for hemipelagic mud samples from the Hydrothermal Transition Transect (Sites 1023, 1024, and 1025), the Buried Basement Transect (Sites 1028, 1029, 1030, and 1031), and the Rough Basement Transect (Sites 1026 and 1027). See Figure 3 for descriptions of lithostratigraphic units. Dashed vertical lines correspond to mean values for each mineral group.

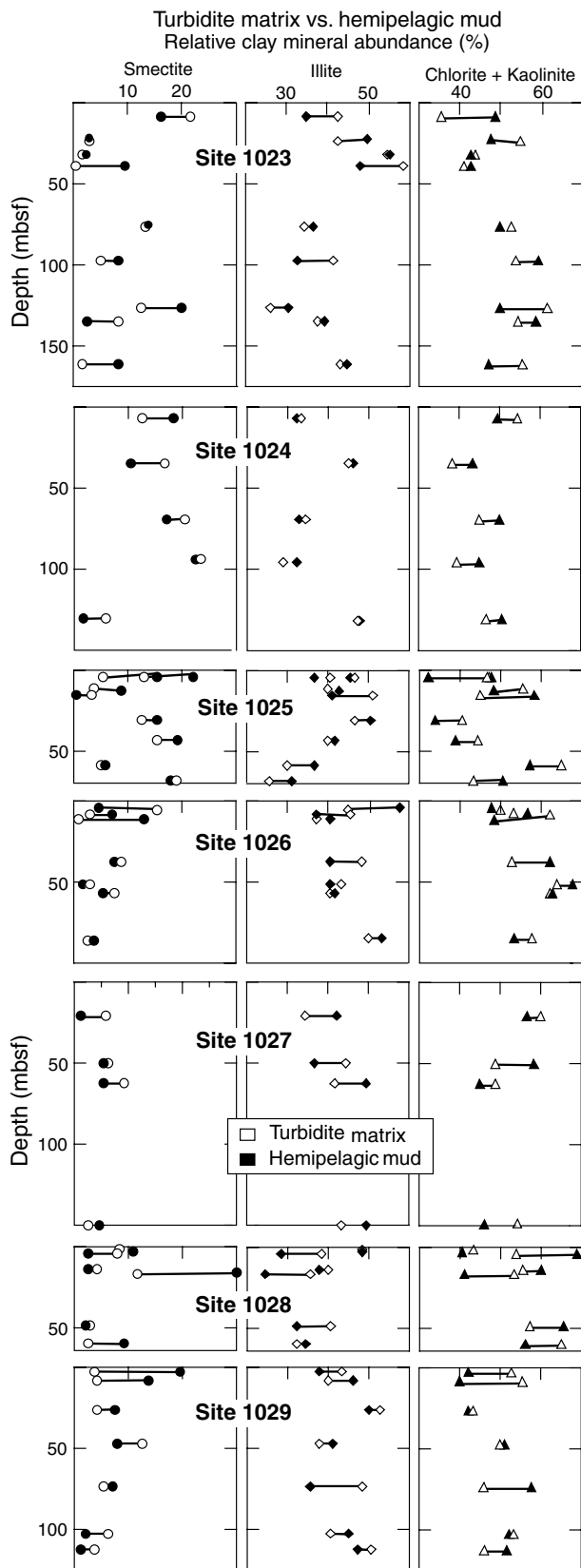


Figure 8. Contrasts between relative abundance of smectite, illite, and chlorite + kaolinite (<2- μ m-size fraction) for sample pairs of hemipelagic mud and turbidite matrix, Sites 1023 through 1029. Note that shifts in mineralogy are not systematic with respect to lithology. See Table 6 (on CD-ROM, back pocket, this volume) for all data values.

contain relatively high contents of smectite, as might be expected with widespread chemical weathering of volcanic source materials; the average smectite content in Bonneville reservoir is 55%, with individual values as high as 86% (Knebel et al., 1968). Artificial compartmentalization of this fluvial system by dam construction probably has less effect on downstream changes in suspended sediment composition than it does on bedload composition, so the mean value of 55% may be a reasonable estimate for the integrated basin-wide output. Tributaries in the lower Columbia River basin contain an even higher average of 89% smectite (Knebel et al., 1968). More significantly, perhaps, offshore studies by Duncan et al. (1970) and Karlin (1980) showed that smectite content decreases across the continental margin, from over 50% to less than 20%, with increasing distance from the Columbia River mouth. Griggs and Kulm (1970) also found that the Holocene clays funneled south through Cascadia Channel are enriched in smectite (average = 52%) relative to nearby Pleistocene deposits in southern Cascadia Basin (average = 37%). These differences may have occurred because of shifts in the contributions from different Columbia River sub-basins during glacial-interglacial cycles (Griggs and Kulm, 1970). Another contributing factor might have been differences in the balance between mechanical and chemical weathering during glacial-interglacial cycles.

One of our unexpected discoveries is the low content of detrital smectite throughout the study area. Working with surface cores from nearby sites, Carson and Acaro (1983) also documented low contents of smectite (typically <20% in size fractions <0.5 μ m), but the average for our Pleistocene and Pliocene mud samples is a scant 8% smectite (Table 2). This shift in clay mineralogy, relative to Columbia River output, indicates that the extent of chemical alteration of volcanic rocks and pyroclastic deposits in the detrital source areas was minor. The predominance of chlorite-rich muds (mean value of chlorite + kaolinite is 52%) indicates, instead, that the source regions were subjected to rapid mechanical weathering, particularly glacial erosion. Source terrains probably included polymictic mixtures of sedimentary, metamorphic, and igneous lithologies. Clay-mineral suites are nearly identical in the intensely glaciated fjords, inlets, and shelf environments of southern Alaska (Molnia and Hein, 1982; Naidu and Mowatt, 1983), as well as along the continental margin of southern Oregon and northern California, where volcanic input is also lower (Griggs and Hein, 1980; Karlin, 1980).

Regional Patterns of Sediment Dispersal

Quaternary sand samples from the Astoria Fan system are broadly similar to those recovered during ODP Leg 168 (Fig. 9). On the other hand, clay-mineral suites from the Columbia River are significantly enriched in smectite relative to the mud samples from the Leg 168 sites. Evidently, surface currents spread the muddy Columbia River discharge toward the north, but the plume becomes diluted or redirected as it reaches the Washington slope and moves downslope into the northwest portion of Cascadia Basin (Carson and Acaro, 1983). Most of the Columbia River sediment is funneled through Quinalt, Willapa, and Astoria Canyons, then directed south across the Astoria Fan system (Duncan and Kulm, 1970; Baker, 1976). Accordingly, despite similar detrital modes, we conclude that the Columbia River has not been the principle source for Pliocene and Pleistocene sediments in the Leg 168 study area. A mixed source is more likely, with potential contributions from Vancouver Island, the Olympic Peninsula, and perhaps western British Columbia via the Fraser River and Strait of Juan de Fuca. Lithologic similarities among those terrains, especially when combined with the likely effects of glacial homogenization and postglacial recycling, precludes additional refinement of provenance. As a final point, we acknowledge that our interpretation is difficult to reconcile with previous explanations for the more lithic-rich Pliocene petrofacies beneath Astoria Fan (Scheidegger et al., 1973; Marsaglia and Ingersoll, 1992). Vancouver Island probably was not the source for the Pliocene petrofacies at Site 174;

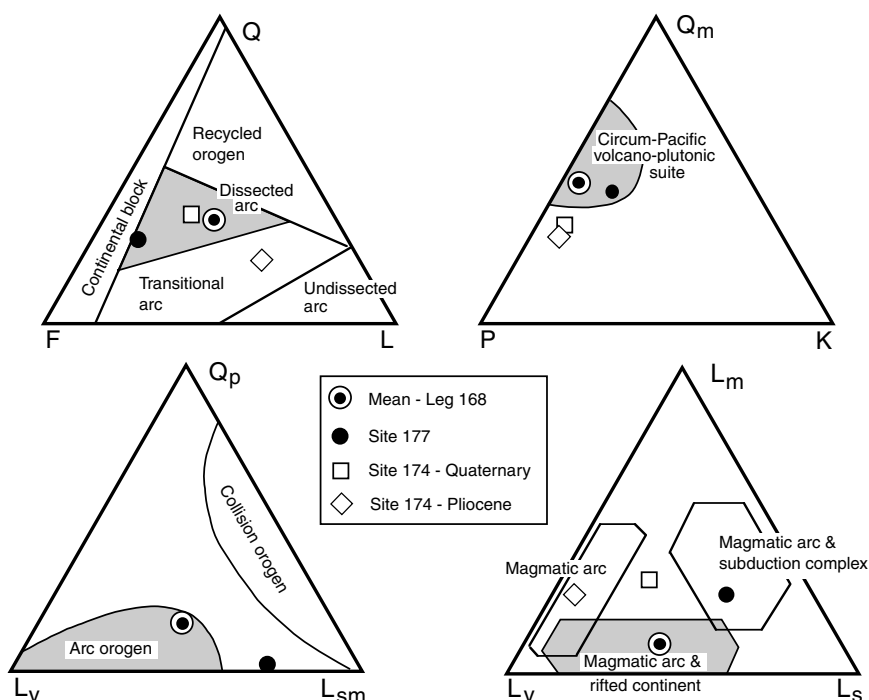


Figure 9. Ternary diagrams showing a comparison among mean detrital modes for sand deposits from the Leg 168 study area (from Saettler, 1998), Site 174 of the DSDP (from Marsaglia and Ingersoll, 1992), and Site 177 of the DSDP (from Gergen and Ingersoll, 1986). Q = total quartz; F = total feldspar; L = unstable lithic fragments; Q_m = monocrystalline quartz; P = plagioclase; K = potassium feldspar; Q_p = polycrystalline quartz; L_v = volcanic-rock fragments; L_{sm} = sedimentary-rock and metasedimentary-rock fragments; L_m = metamorphic-rock fragments. Boundaries for tectonic provenance fields are from Dickinson and Suczek (1979), Dickinson et al. (1983), and Ingersoll and Suczek (1979).

the Klamath Mountains may be a more viable alternative, as suggested by Scheidegger et al. (1973).

Judging from regional bathymetry, several overlapping pathways probably carried individual turbidity currents into the Leg 168 corridor of Cascadia Basin. The first path begins with small submarine canyons that are incised into the western margin of Vancouver Island and continues via Vancouver Valley (Fig. 1). Given the corridor's north- to northeast-striking fabric of basement structures, it seems likely that some of the sandy sediments were transported southward through the Vancouver Valley and Juan de Fuca Channel system. This interpretation is also supported by the seismic-reflection expression of small channel-levee features within the Hydrothermal Transition Transect (Shipboard Scientific Party, 1997a). The second main pathway is through Barkley, Nitinat, and Juan de Fuca Canyons, all of which discharge near the apex of Nitinat Fan (Fig. 1). These canyons connect upstream to the Strait of Juan de Fuca, and their discharge flows around the northern margin of the fan. Nitinat Valley directs turbidity currents westward into Vancouver Valley just north of Sites 1026 and 1027 (Fig. 1). Another contribution, indistinguishable from the Nitinat Valley input, might be unconfined turbidity currents that spread across the northern part of Nitinat Fan. At the northwestern fan fringe, such sheet flows should either spill into Vancouver Valley or deflect toward the south in response to the basement fabric.

Implications of Strike-Parallel Changes in Clay Mineralogy

Smectite-group minerals play a crucial role in the fluid budgets and mechanical behavior of subduction margins (Vrolijk, 1990). The dehydration reaction of smectite to illite, for example, may be largely responsible for the freshening of pore waters within such systems as Nankai Trough and Barbados Ridge (Kastner et al., 1991, 1993; Vrolijk et al., 1991; Bekins et al., 1995). In addition, clay minerals of the smectite group are mechanically weak (e.g., Wang, 1980; Morrow et al., 1982; Bird, 1984; Logan and Rauenzahn, 1987). As diagenesis progresses with increasing temperature and depth, clay-mineral suites should become increasingly depleted in smectite (Hower et al., 1976; Bruce, 1984). The sedimentary section, consequently, should strengthen with depth because of concomitant increases in the

coefficient of internal friction. At the same time, decreases in shear strength may occur locally because of the buildup of excess pore-water pressure and migration of fluids into fault zones (Moore and Vrolijk, 1992; Shipley et al., 1994; Moore et al., 1995). In the cases of both Cascadia and Nankai Trough, the transition from stable-sliding to stick-slip behavior along the basal décollement of the accretionary prism may be governed by the smectite-to-illite diagenetic front (Hyndman and Wang, 1993; Hyndman et al., 1995). This important hypothesis needs to be evaluated thoroughly within the context of strike-parallel zonation of clay mineralogy, particularly as documented outboard of the Cascadia subduction front. Based on the data discussed above, sediments near the Columbia River mouth probably start off with enough detrital smectite (>50% of the <2- μ m-size fraction) to affect fluid budgets and physical properties substantially as they pass through the subduction front and diagenesis progresses in the deeper subsurface. On the other hand, smectite content decreases markedly toward the Strait of Juan de Fuca, reaching an average value of only 8% within the Leg 168 study area. Diagenetic changes of smectite-poor clay-mineral suites should be much more subtle, and such small shifts in mineralogy should not alter material properties significantly within (or below) the Vancouver corridor of the accretionary prism.

CONCLUSIONS

The major conclusions of our compositional study of Cascadia Basin sediments are as follows.

1. Sand-sized grains from turbidites are compositionally homogeneous, both within and among the Leg 168 sites. Average detrital modes are $Q = 35$, $F = 35$, and $L = 30$; $Q_m = 46$, $P = 49$, and $K = 5$; $Q_p = 16$, $L_v = 43$, and $L_{sm} = 41$; and $L_v = 52$, $L_s = 39$, and $L_m = 9$. The generic source for these sands was a polymictic dissected arc.
2. Relative abundance of clay minerals are similar for turbidite matrix and interbeds of mud; there are no systematic shifts in mineralogy as a function of the lithologic host. Average mineral abundance for mud deposits are smectite = 8%, illite =

40%, and chlorite + kaolinite = 52%. Clay-mineral source areas probably included igneous, metamorphic, and sedimentary rocks, plus reworked glacial deposits enriched in detrital chlorite. We attribute the erratic stratigraphic changes in clay mineralogy to surface currents, near-bottom nepheloid clouds, and low-density turbidity currents converging from several directions, as well as subtle changes imparted by glacial vs. interglacial weathering.

3. Site-specific detrital sources included Vancouver Island and the Olympic Peninsula. Sediment discharge from the west coast of Vancouver Island probably moved south through Vancouver Valley. Detritus from southern Vancouver Island and the Olympic Peninsula (and perhaps the Fraser River drainage) moved toward Cascadia Basin via the Strait of Juan de Fuca. Turbidity currents and nepheloid-layer suspensions flowed down Barkley, Nitinat, and Juan de Fuca Canyons, spread over the northern apex of Nitinat fan, and then merged and mixed with Vancouver Valley sediments moving from the north.
4. Detrital smectite decreases significantly toward the north as one moves away from the mouth of the Columbia River. This zonation in clay mineralogy probably contributes to complicated three-dimensional changes in diagenesis, fluid budgets, and physical properties inboard of the Cascadia subduction front. Smectite content near the Leg 168 study area appears to be too low, however, to have a measurable effect on the material properties of strata as they undergo diagenesis and deformation within (or below) the adjacent accretionary prism.

ACKNOWLEDGMENTS

We thank the crew and technical staff of *JOIDES Resolution* for their help in obtaining the samples used in this study. Brandon Gomer and Amanda Cavin assisted in the laboratory. This paper represents the distillation of a M.S. thesis completed by Kimberly (Saettler) Hoke. Funding was provided by the U.S. Science Support Program, Grant 168-F000503. Richard Behl provided a helpful review of the manuscript.

REFERENCES

- Baker, E.T., 1976. Distribution, composition, and transport of suspended particulate matter in the vicinity of Willapa submarine canyon, Washington. *Geol. Soc. Am. Bull.*, 87:625–632.
- Baker, E.T., and Hickey, B.M., 1986. Contemporary sedimentation processes in and around an active west coast submarine canyon. *Mar. Geol.*, 71:15–34.
- Barnard, W.D., 1978. The Washington continental slope: Quaternary tectonics and sedimentation. *Mar. Geol.*, 27:79–114.
- Beeson, M.H., and Tolan, T.L., 1990. The Columbia River Basalt Group in the Cascade Range: a middle Miocene reference datum for structural analysis. *J. Geophys. Res.*, 95:19547–19559.
- Bekins, B.A., McCaffrey, A.M., and Driess, S.J., 1995. Episodic and constant flow models for the origin of low-chloride waters in a modern accretionary complex. *Water Resour. Res.*, 31:3205–3215.
- Bird, P., 1984. Hydration-phase diagrams and friction of montmorillonite under laboratory and geologic conditions, with implications for shale compaction, slope stability, and strength of fault gouge. *Tectonophysics*, 107:235–260.
- Biscaye, P.E., 1964. Distinction between kaolinite and chlorite in recent sediments by X-ray diffraction. *Am. Miner.*, 49:1281–1289.
- , 1965. Mineralogy and sedimentation of recent deep-sea clays in the Atlantic Ocean and adjacent seas and oceans. *Geol. Soc. Am. Bull.*, 76:803–832.
- Blakely, R.J., and Jachens, R.C., 1990. Volcanism, isostatic residual gravity, and regional tectonic setting of the Cascade Volcanic Province. *J. Geophys. Res.*, 95:19439–19451.
- Brandon, M.T., Roden-Tice, M.K., and Garver, J.I., 1998. Late Cenozoic exhumation of the Cascadia accretionary wedge in the Olympic Mountains, northwest Washington State. *Geol. Soc. Am. Bull.*, 110:985–1009.
- Bruce, C.H., 1984. Smectite dehydration—its relation to structural development and hydrocarbon accumulation in northern Gulf of Mexico basin. *AAPG Bull.*, 68:673–683.
- Carlson, P.R., and Nelson, C.H., 1969. Sediments and sedimentary structures of the Astoria submarine canyon-fan system, northeast Pacific. *J. Sediment. Petrol.*, 39:1269–1282.
- , 1987. Marine geology and resource potential of Cascadia Basin. In Scholl, D.W., Grantz, A., and Vedder, J.G. (Eds.), *Geology and Resource Potential of the Continental Margin of Western North America and Adjacent Ocean Basins—Beaufort Sea to Baja California*. Circum-Pac. Council. Energy Miner. Res., Earth Sci. Ser., 6:523–535.
- Carson, B., 1971. Stratigraphy and depositional history of Quaternary sediments in Northern Cascadia Basin and Juan de Fuca Abyssal plain, northeast Pacific Ocean [Ph.D. dissert.]. Univ. Washington, Seattle.
- , 1973. Acoustic stratigraphy, structure and history of Quaternary deposition in Cascadia Basin. *Deep Sea Res.*, 20:387–396.
- Carson, B., and Acaro, N.P., 1983. Control of clay-mineral stratigraphy by selective transport in Late Pleistocene-Holocene sediments of northeastern Cascadia Basin-Juan de Fuca Abyssal Plain: implications for studies of clay-mineral provenance. *J. Sediment. Petrol.*, 53:395–406.
- Carson, B., Baker, E.T., Hickey, B.M., Nittrouer, C.A., DeMaster, D.J., Thorbjarnarson, K.W., and Snyder, G.W., 1986. Modern sediment dispersal and accumulation in Quinault submarine canyon: a summary. *Mar. Geol.*, 71:1–13.
- Carson, B., Yuan, J., Myers, P.B., and Barnard, W.D., 1974. Initial deep-sea sediment deformation at the base of the Washington continental slope: a response to subduction. *Geology*, 2:561–564.
- Chamov, N.P., and Murdmaa, I.O., 1995. Coarse fraction minerals of sands in Cascadia Margin sediments. In Carson, B., Westbrook, G.K., Musgrave, R.J., and Suess, E. (Eds.), *Proc. ODP, Sci. Results*, 146 (Pt 1): College Station, TX (Ocean Drilling Program), 33–43.
- Clague, J.J., 1986. Bedrock geology (Canadian Cordillera). In Fulton, R.J. (Ed.), *Quaternary Geology of Canada and Greenland*. Geol. Soc. Am., Geol. of North Am. Ser., K-1:22–25.
- Clague, J.J., Luternauer, J.L., and Hebda, R.J., 1983. Sedimentary environments and postglacial history of the Fraser Delta and lower Fraser Valley, British Columbia. *Can. J. Earth Sci.*, 20:1314–1326.
- Davis, E.E., and Hyndman, R.D., 1989. Accretion and recent deformation of sediments along the northern Cascadia subduction zone. *Geol. Soc. Am. Bull.*, 101:1465–1480.
- Dickinson, W.R., 1970. Interpreting detrital modes of graywacke and arkose. *J. Sediment. Petrol.*, 40:695–707.
- , 1982. Compositions of sandstones in circum-Pacific subduction complexes and fore-arc basins. *AAPG Bull.*, 66:121–137.
- Dickinson, W.R., Beard, L.S., Brakenridge, G.R., Erjavec, J.L., Ferguson, R.C., Inman, K.F., Knepp, R.A., Lindberg, F.A., and Ryberg, P.T., 1983. Provenance of North American Phanerozoic sandstones in relation to tectonic setting. *Geol. Soc. Am. Bull.*, 94:222–235.
- Dickinson, W.R., and Suczek, C.A., 1979. Plate tectonics and sandstone compositions. *AAPG Bull.*, 63:2164–2182.
- Duncan, J.R., and Kulm, L.D., 1970. Mineralogy, provenance, and dispersal history of late Quaternary deep-sea sands in Cascadia Basin and Blanco Fracture zone off Oregon. *J. Sediment. Petrol.*, 40:874.
- Duncan, J.R., Kulm, L.D., and Griggs, G.B., 1970. Clay mineral composition of Late Pleistocene and Holocene sediments of Cascadia Basin, northeastern Pacific Ocean. *J. Geol.*, 78:213–221.
- EEZ Scan 84 Scientific Staff, 1986. *Atlas of the Exclusive Economic Zone, Western Conterminous United States*. U.S. Geol. Surv., Misc. Investigations Ser., I-1972.
- Garrison, R.E., Luternauer, J.L., Grill, E.V., MacDonald, R.D., and Murray, J.W., 1969. Early diagenetic cementation of recent sands, Fraser River delta, British Columbia. *Sedimentology*, 12:27–46.
- Gergen, L.D., and Ingersoll, R.V., 1986. Petrology and provenance of Deep Sea Drilling Project sand and sandstone from the North Pacific Ocean and the Bering Sea. *Sediment. Geol.*, 51:29–56.
- Giambalvo, E.R., Fisher, A.T., Martin, J.T., Darty, L., and Lowell, R.P., in press. Origin of elevated sediment permeability in a hydrothermal seepage zone, eastern flank of the Juan de Fuca Ridge, and implications for transport of fluid and heat. *J. Geophys. Res.*
- Gibbs, R.J., 1977. Clay mineral segregation in the marine environment. *J. Sediment. Petrol.*, 47:237–243.
- Griggs, G.B., Carey, A.G., and Kulm, L.D., 1969. Deep-sea sedimentation and sediment-fauna interaction in Cascadia Channel and on Cascadia abyssal plain. *Deep-Sea Res.*, 16:157–170.

- Griggs, G.B., and Hein, J.R., 1980. Sources, dispersal and clay mineral composition of fine-grained sediment off central and northern California. *J. Geol.*, 88:541–566.
- Griggs, G.H., and Kulm, L.D., 1970. Sedimentation in the Cascadia deep sea channel. *Geol. Soc. Am. Bull.*, 81:1361–1384.
- Halpern, D., Smith, R.L., and Reed, R.K., 1978. On the California Undercurrent over the continental slope off Oregon. *J. Geophys. Res.*, 83:1366–1372.
- Hathon, E.G., and Underwood, M.B., 1991. Clay mineralogy and chemistry as indicators of hemipelagic sediment dispersal south of the Aleutian arc. *Mar. Geol.*, 97:145–166.
- Herzer, R.H., 1978. Submarine canyons and slumps on the continental slope off southern Vancouver Island. *Geol. Surv. Can. Curr. Res.*, 78-1A:357–360.
- Hickey, B., Baker, E., and Kachel, N., 1986. Suspended particle movement in and around Quinault submarine canyon. *Mar. Geol.*, 71:35–83.
- Houghton, H.F., 1980. Refined techniques for staining plagioclase and alkali feldspars in thin section. *J. Sediment. Petrol.*, 50:629–931.
- Hower, J., Eslinger, E.V., Hower, M.E., and Perry, E.A., 1976. Mechanism of burial metamorphism of argillaceous sediment. 1. Mineralogical and chemical evidence. *Geol. Soc. Am. Bull.*, 87:725–737.
- Huyer, A., 1983. Coastal upwelling in the California Current system. *Prog. Oceanogr.*, 8:259–284.
- Hyndman, R.D., and Wang, K., 1993. Thermal constraints on the zone of major thrust earthquake failure: the Cascadia subduction zone. *J. Geophys. Res.*, 98:2039–2060.
- Hyndman, R.D., Wang, K., and Yamano, M., 1995. Thermal constraints on the seismogenic portion of the southwestern Japan subduction thrust. *J. Geophys. Res.*, 100:15373–15392.
- Hyndman, R.D., Yorath, C.J., Clowes, R.M., and Davis, E.E., 1990. The northern Cascadia subduction at Vancouver Island: seismic structure and tectonic history. *Can. J. Earth Sci.*, 27:313–319.
- Ingersoll, R.V., Bullard, T.F., Ford, R.L., Grimm, J.P., Pickle, J.D., and Sares, S.W., 1984. The effect of grain size on detrital modes: a test of the Gazzidickinson point-counting method. *J. Sediment. Petrol.*, 54:103–116.
- Ingersoll, R.V., and Suczek, C.A., 1979. Petrology and provenance of Neogene sand from Nicobar and Bengal Fans, DSDP Sites 211 and 218. *J. Sediment. Petrol.*, 49:1217–1228.
- Karl, H.A., Hampton, M.A., and Kenyon, N.H., 1989. Lateral migration of Cascadia Channel in response to accretionary tectonics. *Geology*, 17:144–147.
- Karlin, R., 1980. Sediment sources and clay mineral distributions off the Oregon coast. *J. Sediment. Petrol.*, 50:543–560.
- Kastner, M., Elderfield, H., Jenkins, W.J., Gieskes, J.M., and Gamo, T., 1993. Geochemical and isotopic evidence for fluid flow in the western Nankai subduction zone, Japan. In Hill, I.A., Taira, A., Firth, J.V., et al., *Proc. ODP, Sci. Results*, 131: College Station, TX (Ocean Drilling Program), 397–413.
- Kastner, M., Elderfield, H., and Martin, J.B., 1991. Fluids in convergent margins: what do we know about their composition, origin, role in diagenesis and importance for oceanic chemical fluxes? *Philos. Trans. R. Soc. London A*, 335:243–259.
- Kirwan, A.D., McNally, G.J., Reyna, E., and Merrell, W.J., 1978. The near-surface circulation of the Eastern North Pacific. *J. Phys. Oceanogr.*, 8:937.
- Knebel, H.J., Kelly, J.C., and Whetten, J.T., 1968. Clay minerals of the Columbia River: a qualitative, quantitative and statistical evaluation. *J. Sediment. Petrol.*, 38:600–611.
- Logan, J.M., and Rauenzahn, K.A., 1987. Frictional dependence of gouge mixtures of quartz and montmorillonite on velocity, composition and fabric. *Tectonophysics*, 144:87–108.
- Lynn, R.J., and Simpson, J.J., 1987. The California Current system: the seasonal variability of its physical characteristics. *J. Geophys. Res.*, 92:12947–12966.
- Marsaglia, K.M., and Ingersoll, R.V., 1992. Compositional trends in arc-related, deep-marine sand and sandstone: a reassessment of magmatic-arc provenance. *Geol. Soc. Am. Bull.*, 104:1637–1649.
- Mayers, I.R., and Bennett, L.C., 1973. Geology of the Strait of Juan de Fuca. *Mar. Geol.*, 15:89–117.
- McBirney, A.R., 1978. Volcanic evolution of the Cascade Range. *Annu. Rev. Earth Planet. Sci.*, 6:437–456.
- Molnia, B.F., and Hein, J.R., 1982. Clay mineralogy of a glacially dominated, subarctic continental shelf: northeastern Gulf of Alaska. *J. Sediment. Petrol.*, 52:515–528.
- Moore, D.M., and Reynolds, R.C., Jr., 1997. *X-ray Diffraction and the Identification and Analysis of Clay Minerals*: Oxford (Oxford Univ. Press).
- Moore, J.C., Shipley, T.H., Goldberg, D., Ogawa, Y., Filice, F., Fisher, A., Jurado, M.-J., Moore G.F., Rabaute, A., Yin, H., Zwart, G., and Brueckmann, W., Henry, P., Ashi, J., Blum, P., Meyer, A., Housen, B., Kastner, M., Labaume, P., Laier, T., Leitch, E.C., Maltman, A.J., Peacock, S., Steiger, T.H., Tobin, H.J., Underwood, M.B., Xu, Y., Zheng, Y., 1995. Abnormal fluid pressures and fault zone dilation in the Barbados accretionary prism: evidence from logging while drilling. *Geology*, 23:605–608.
- Moore, J.C., and Vrolijk, P., 1992. Fluids in accretionary prisms. *Rev. Geophys.*, 30:113–135.
- Morrow, C.A., Shi, L.Q., and Byerlee, J.D., 1982. Strain hardening and strength of clay-rich fault gouges. *J. Geophys. Res.*, 87:6771–6780.
- Muller, J.E., 1977. Evolution of the Pacific Margin, Vancouver Island, and adjacent regions. *Can. J. Earth Sci.*, 14:2062–2085.
- Naidu, A.S., and Mowatt, T.C., 1983. Sources and dispersal patterns of clay minerals in surface sediments from the continental-shelf areas off Alaska. *Geol. Soc. Am. Bull.*, 94:841–854.
- Nelson, C.H., 1976. Late Pleistocene and Holocene depositional trends, processes and history of Astoria deep-sea fan, northeast Pacific. *Mar. Geol.*, 20:129–173.
- Nelson, C.H., Carlson, P.R., Byrne, J.V., and Alpha, T.R., 1970. Development of the Astoria canyon-fan physiography and comparison with similar systems. *Mar. Geol.*, 8:259–291.
- Pharo, C.H., and Barnes, W.C., 1976. Distribution of surficial sediments of the central and southern Strait of Georgia, British Columbia. *Can. J. Earth Sci.*, 13:684–696.
- Reid, R.K., and Halpern, D., 1976. Observation of the California Undercurrent off Washington and Vancouver Island. *Limnol. Oceanogr.*, 21:389–398.
- Saettler, K.D., 1998. Composition, provenance, and depositional patterns of turbidites and hemipelagic muds, northwestern Cascadia Basin [M.S. thesis]. Univ. Missouri, Columbia.
- Scheidegger, K.F., Kulm, L.D., and Piper, D.J.W., 1973. Heavy mineralogy of unconsolidated sands in northeastern Pacific sediments: Leg 18, Deep Sea Drilling Project. In Kulm, L.D., von Huene, R., et al., *Init. Repts. DSDP*, 18: Washington (U.S. Govt. Printing Office), 877–888.
- Shipboard Scientific Party, 1997a. Buried basement transect (Sites 1028, 1029, 1030, 1031, and 1032). In Davis, E.E., Fisher, A.T., Firth, J.V., et al., *Proc. ODP, Init. Repts.*, 168: College Station, TX (Ocean Drilling Program), 161–212.
- , 1997b. Hydrothermal transition transect (Sites 1023, 1024, and 1025). In Davis, E.E., Fisher, A.T., Firth, J.V., et al., *Proc. ODP, Init. Repts.*, 168: College Station, TX (Ocean Drilling Program), 49–100.
- , 1997c. Introduction and summary: hydrothermal circulation in the oceanic crust and its consequences on the eastern flank of the Juan de Fuca Ridge. In Davis, E.E., Fisher, A.T., Firth, J.V., et al., *Proc. ODP, Init. Repts.*, 168: College Station, TX (Ocean Drilling Program), 7–21.
- , 1997d. Leg 167 introduction. In Lyle, M., Koizumi, I., Richter, C., et al., *Proc. ODP, Init. Repts.*, 167: College Station, TX (Ocean Drilling Program), 5–13.
- , 1997e. Rough basement transect (Sites 1026 and 1027). In Davis, E.E., Fisher, A.T., Firth, J.V., et al., *Proc. ODP, Init. Repts.*, 168: College Station, TX (Ocean Drilling Program), 101–160.
- Shipley, T.H., Moore, G.F., Bangs, N.L., Moore, J.C., and Stoffa, P.L., 1994. Seismically inferred dilatancy distribution, northern Barbados Ridge décollement: implications for fluid migration and fault strength. *Geology*, 22:411–414.
- Stokke, P.R., Carson, B., and Baker, E.T., 1977. Comparison of the bottom nepheloid layer and late Holocene deposition on Nitinat Fan: implications for lutite dispersal and deposition. *Geol. Soc. Am. Bull.*, 8:1586–1592.
- Tabor, R.W., and Cady, W.M., 1978. The structure of the Olympic Mountains, Washington—analysis of a subduction zone. *Geol. Surv. Prof. Pap. U.S.*, 1033.
- Thorbjarnarson, K.W., Nittrouer, C.A., and DeMaster, D.J., 1986. Accumulation of modern sediment in Quinault submarine canyon. *Mar. Geol.*, 71:107–124.
- Underwood, M.B., 1986. Transverse infilling of the Central Aleutian Trench by unconfined turbidity currents. *Geo-Mar. Lett.*, 6:7–13.
- Underwood, M.B., Orr, R., Pickering, K., and Taira, A., 1993. Provenance and dispersal patterns of sediments in the turbidite wedge of Nankai

- Trough. In Hill, I.A., Taira, A., Firth, J.V., et al., *Proc. ODP, Sci. Results*, 131: College Station, TX (Ocean Drilling Program), 15–34.
- Vrolijk, P., 1990. On the mechanical role of smectite in subduction zones. *Geology*, 18:703–707.
- Vrolijk, P., Fisher, A., and Gieskes, J., 1991. Geochemical and geothermal evidence for fluid migration in the Barbados accretionary prism (ODP Leg 110). *Geophys. Res. Lett.*, 18:947–950.
- Wang, C.-Y., 1980. Sediment subduction and frictional sliding in a subduction zone. *Geology*, 8:530–533.
- Whetten J.T., Kelley, J.C., and Hanson, L., 1969. Characteristics of Columbia River sediment transport. *J. Sediment. Petrol.*, 39:1149.
- White, S.M., 1970. Mineralogy and geochemistry of continental shelf sediments off the Washington-Oregon coast. *J. Sediment. Petrol.*, 40:38–54.

Date of initial receipt: 7 December 1998

Date of acceptance: 27 September 1999

Ms 168SR-012